

Strictly local Union–Find

Tim Chan¹ and Simon C. Benjamin^{1,2}

¹Department of Materials, University of Oxford, Parks Road, Oxford OX1 3PH, United Kingdom

²Quantum Motion, 9 Sterling Way, London N7 9HJ, United Kingdom

June 8, 2023

Fault-tolerant quantum computing requires classical hardware to perform the decoding necessary for error correction. The Union–Find decoder is one of the best candidates for this. It has remarkably organic characteristics, involving the growth and merger of data structures through nearest-neighbour steps; this naturally suggests the possibility of realising Union–Find using a lattice of simple processors with strictly nearest-neighbour links. In this way the computational load can be distributed with near-ideal parallelism. Here we build on earlier work to show for the first time that this strict (rather than partial) locality is practical, with a worst-case runtime $\mathcal{O}(d^3)$ and mean runtime subquadratic in d where d is the surface code distance. A novel parity-calculation scheme is employed, which can also simplify previously proposed architectures. We compare our strictly local realisation with one augmented by long-range links; while the latter is of course faster, we note that local asynchronous logic could negate the difference.

1 Introduction

In the fault-tolerant era of quantum computing, the quantum hardware must be supported by classical decoders that infer the nature of errors ‘on the fly’ from measurements. It is challenging to find decoder implementations that are sufficiently fast, compact, and (ideally) with low power requirements. We focus on decoders for the *surface code* [5, 9, 16]: one of the most promising error-correcting codes needed for fault tolerance due to its simplicity. Many decoders have been developed such as *minimum-weight perfect matching* (MWPM) [8, 10], *renormalisation group* [6, 7], *Markov chain Monte Carlo* [27], and various using *belief propagation* [1, 12, 13, 15] and *neural networks* [20, 23]. A recent development is the *hierarchical decoder* [2, 18, 21, 25] in which a simple, partially capable decoder handles most of the decoding, sending the trickier problems to a more complex decoder.

Tim Chan: timothy.chan@materials.ox.ac.uk

Simon C. Benjamin: simon.benjamin@materials.ox.ac.uk

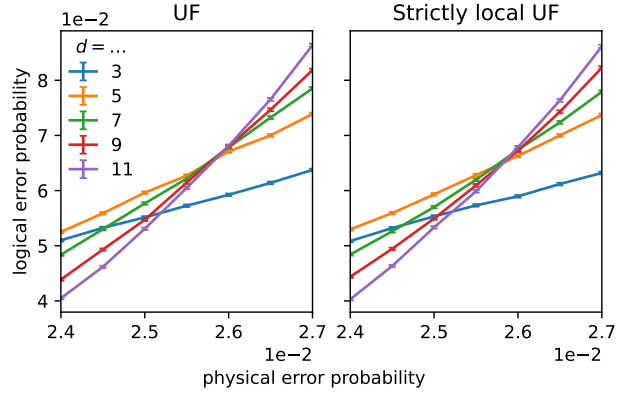


Figure 1: Threshold plots for original and strictly local UF. We use the phenomenological noise model and set measurement error to physical error probability. Each datapoint is the mean of 10^6 samples of decoding cycle, with errorbars showing standard error. The threshold is the physical error probability at which the lines cross, $\sim 2.58 \cdot 10^{-2}$ for both plots; for UF this is consistent with previous literature [14, §5.4]. The $d = 3$ line misses the crossing point as it is heavily affected by boundary effects (it is such a small code, the size of its boundary is comparable to the size of its bulk).

One simple and fast but fully capable decoder is the Union–Find decoder (UF) designed by Delfosse et al. [3, 4]. It has a relatively high accuracy and a mean runtime slightly higher than cubic in d [17, §2.3]. Liyanage et al. [17] recently proposed *Helios*, the FPGA implementation of an almost-local version of UF. By *local* we mean runnable on a grid of identical nodes (classical processors), each communicating only with their nearest neighbours. Helios is local save for an additional controller which communicates with each node directly. They report an improved mean runtime: sublinear in d .

Our main results extend this literature, especially the ideas proposed for Helios, as we introduce a paradigm which reduces the memory requirements of each node, the number and size of messages passed around, the complexity of the grid architecture, and the number of stages in the algorithm as a whole. This improvement is a simple scheme inspired by anyon annihilation to calculate parities. Moreover we also design a *strictly local* version of UF (SLUF), the first of its kind, which is even more practical due to the

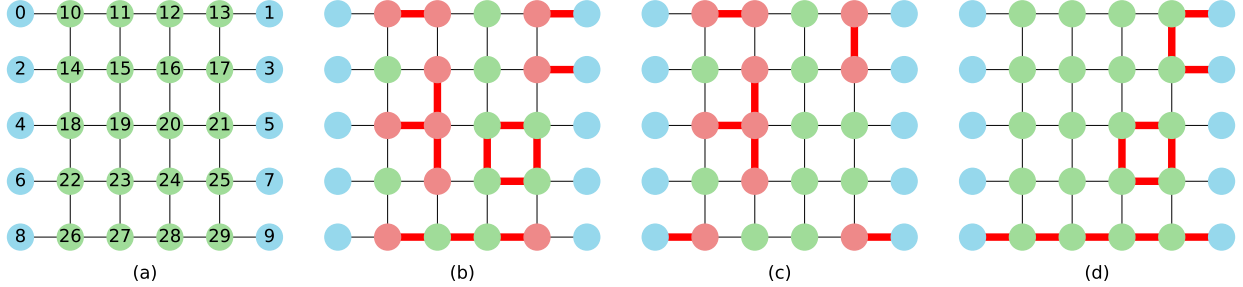


Figure 2: (a) The graph representing a distance-5 surface code. Bulk nodes are green; boundary nodes, blue. (b) An example of an error \mathbb{E} is the set of red edges whose corresponding syndrome \mathbb{S} is the set of red nodes. Note a path in \mathbb{E} (like that from node 26 to 29) will make a defect only at each endpoint; a cycle will make no defects. The decoder sees only \mathbb{S} , not \mathbb{E} . (c) A correction \mathbb{C} for \mathbb{E} is the set of red edges. The syndrome made by \mathbb{C} is always the same as that of \mathbb{E} . (d) The leftover \mathbb{L} after combining \mathbb{E} and \mathbb{C} . This example comprises a cycle and two paths: one between nodes on the same boundary and one between opposite boundaries. The latter represents a logical bitflip.

lack of long-range links, and whose mean runtime is subquadratic in d for error probabilities below threshold. Having compared these almost- and strictly local models we note that the use of a fast communication relay implemented with asynchronous logic would constitute a third version of UF which rivals the speed of almost-local UF whilst maintaining strict locality.

As well as having improved mean and worst-case runtime scalings, all three of our versions are just as accurate as original UF. We show this empirically in Fig. 1, noting our versions behave identically in their output.

The paper proceeds as follows. In Section 2 we cover the prerequisite background theory. In Section 3 we discuss almost-local UF as introduced in the Helios scheme and describe our variation of this idea, before describing SLUF in detail in Section 4. We evaluate runtime for both versions of UF in Section 5 and discuss how SLUF can be sped up using asynchronous logic in Section 6. Section 7 concludes.

2 Background

Section 2.1 covers the surface code with a focus on decoding. We approach this standard material using graph theory as it facilitates a natural explanation of UF presented in Section 2.2.

2.1 Surface Code and Decoding

As its name suggests, the surface code arranges the physical qubits on a 2D grid. It encodes one logical qubit and corrects for both bit- and phaseflip errors (the ability to correct these two discrete errors allows us to correct any qubit error [19, §10.3.1]). Here, we describe how to correct bitflip errors; phaseflip errors are corrected analogously. We explain the decoding cycle assuming measurements to be perfect in Section 2.1.1 before generalising to faulty measurements in Section 2.1.2, using the *phenomenological*

noise model [14, §2.3.3].

2.1.1 Perfect Measurements

The surface code is based on the graph $G = (V, E)$ in Fig. 2(a) which comprises a set $V = V_{\text{bulk}} \cup V_{\text{boundary}}$ of nodes arranged on a $d \times (d + 1)$ grid and a set E of edges. Members of V_{bulk} are called bulk nodes; V_{boundary} , boundary nodes. Each edge corresponds to a set of two nodes from V . Physically, each bulk node represents an ancilla qubit used for measurement (sometimes called a *measure qubit*) while each edge represents a data qubit. Boundary nodes represent nothing physical but exist just to allow every data qubit to be represented by an edge. We will treat the decoding problem abstractly in terms of nodes and edges. In a decoding cycle:

1. **Noise corrupts our system:** Each edge bitflips with some probability p called the *physical error probability* i.e. is assigned bit value 1 with probability p , and bit value 0 otherwise. The *error* $\mathbb{E} \subseteq E$ is the set of bitflipped edges.
2. **Ancilla qubits flag the noise:** Every bulk node records the parity of the edges in \mathbb{E} which are incident to it. If it records odd parity, it is a *defect*. The *syndrome* $\mathbb{S} \subseteq V_{\text{bulk}}$ is the set of defects. Figure 2(b) shows an error and its syndrome. Mathematically, $\mathbb{S} = \sigma(\mathbb{E})$ where

$$\sigma(\mathbb{E}) := V_{\text{bulk}} \cap \bigtriangleup_{e \in \mathbb{E}} e \quad (1)$$

and $\bigtriangleup_{e \in \mathbb{E}} e := f \bigtriangleup \dots \bigtriangleup g$ for $\mathbb{E} = \{f, \dots, g\}$ where \bigtriangleup denotes symmetric difference.

3. **The classical decoder acts:** Given \mathbb{S} , the decoder must output a *correction* $\mathbb{C} \subseteq E$ which, if treated as an error, would make the same syndrome \mathbb{S} . In other words, \mathbb{C} must satisfy $\sigma(\mathbb{C}) = \mathbb{S}$. Figure 2(c) shows a correction.

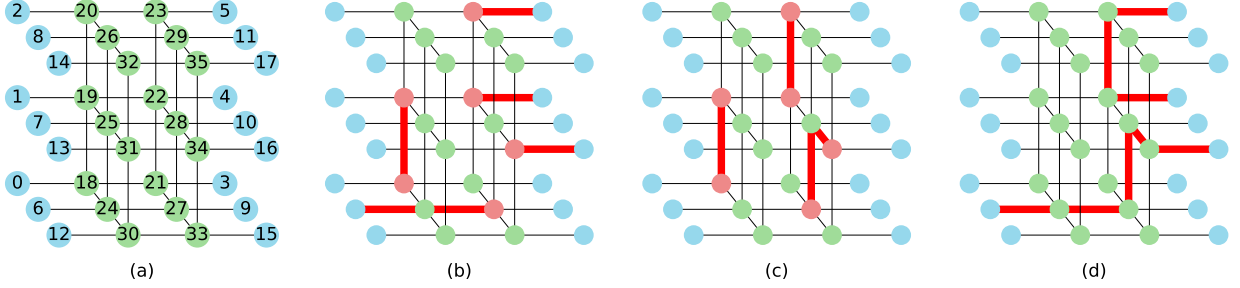


Figure 3: The 3D generalisation of Fig. 2 to account for faulty measurements. (a) Instead of distance-5, we show a distance-3 code for visual clarity. The time axis points upward. (b) The error \mathbb{E} can now include vertical ‘timelike’ edges like that from node 18 to 19. The syndrome \mathbb{S} is the set of red nodes throughout the whole lattice. (c) A correction \mathbb{C} for \mathbb{E} . (d) The leftover \mathbb{L} comprises one path between the same boundary and one between opposite boundaries. The latter represents a logical bitflip.

4. **Success or failure:** The leftover $\mathbb{L} := \mathbb{E} \Delta \mathbb{C}$ is then guaranteed to satisfy the following Lemma (for completeness, a proof is given in Appendix A).

Lemma 1. \mathbb{L} comprises only cycles or paths between distinct boundary nodes.

The question of whether the decoder has been successful depends on whether a logical error has resulted from the correction. Any path between opposite boundaries represents a logical bitflip. Hence, if \mathbb{L} has an odd number of such paths the logical qubit has picked up a logical error. Figure 2(d) shows a leftover with one such path.

The aim of the decoder is to output a correction which is least likely to lead to a logical error. Fig. 1 shows examples of how, for a surface code decoder, logical error probability depends on both d and p . Each decoder has a different *threshold* i.e. physical error probability p_{th} below (above) which increasing d decreases (increases) the logical error probability. The further below threshold a decoder operates, the more effective it is. In the case of UF, operating at its threshold is practically useless; significant benefits of error correction are reaped only when p is several times below threshold i.e. $p \ll p_{\text{th}}$.

2.1.2 Faulty Measurements

In reality, ancilla qubit measurement is faulty i.e. in step 2 each bulk node records the *wrong* parity with some probability q . The result is that the syndrome is subject to some noise: $\mathbb{S} = \sigma(\mathbb{E}) \Delta \mathbb{F}$, where $\mathbb{F} \subseteq V_{\text{bulk}}$ is the set of nodes which record the wrong parity for that measurement round. Note boundary nodes cannot be in \mathbb{F} as they do not represent ancilla qubits which are measured.

The usual way to account for faulty measurements is to measure each ancilla qubit not once but $\tau + 1$ times per decoding cycle, where $\tau > 0$ (intuitively, the higher q is, the higher we should make τ). We

then have not one 2D sheet of syndrome data as in Fig. 2(b), but $\tau + 1$ of them, which we label $\{\mathbb{S}_0, \dots, \mathbb{S}_\tau\}$. In general there is a new \mathbb{E} and \mathbb{F} for each sheet, but the data is cumulative in \mathbb{E} i.e.

$$\mathbb{S}_t = [\bigtriangleup_{u=0}^t \sigma(\mathbb{E}_u)] \Delta \mathbb{F}_t \quad \forall t \in 0.. \tau \quad (2)$$

so to localise each \mathbb{E}_t we take the difference between consecutive sheets:

$$\begin{aligned} \Delta \mathbb{S}_t &:= \mathbb{S}_t \Delta \mathbb{S}_{t-1} \quad \forall t \in 1.. \tau \\ &\stackrel{(2)}{=} \sigma(\mathbb{E}_t) \Delta \mathbb{F}_t \Delta \mathbb{F}_{t-1}. \end{aligned} \quad (3)$$

We can then stack these 2D ‘difference sheets’ $\{\Delta \mathbb{S}_1, \dots, \Delta \mathbb{S}_\tau\}$ to make a 3D simple cubic lattice as in Fig. 3(a). Sheets are stacked such that $\Delta \mathbb{S}_1$ is on the bottom, $\Delta \mathbb{S}_2$ is the next one above, etc. This way, sheets which derive from later measurements are higher up the stack so we can interpret the upward direction as going forward in time (hence the subscript t).

Each bulk node no longer represents a single ancilla qubit; rather, the difference between two consecutive measurements of that ancilla qubit at a given point in time. Each horizontal edge no longer represents a single data qubit but a possible time at which that data qubit could bitflip. Vertical edges are a new addition: each one represents a single possible faulty measurement. Specifically, each edge between $\Delta \mathbb{S}_t$ and $\Delta \mathbb{S}_{t+1}$ corresponds to a possible member of \mathbb{F}_t . This makes sense e.g. a member of \mathbb{F}_1 effects a change in both $\Delta \mathbb{S}_1$ and $\Delta \mathbb{S}_2$ as per Eq. (3).

If we redefine G as this 3D simple cubic lattice, all steps of the decoding cycle are the same as in Section 2.1 with the modification in step 1 that each *horizontal* edge bitflips with probability p ; each *vertical* edge, q . Figure 3(b-d) shows a decoding cycle example.

In our numerical emulations we make two simplifications:

1. We assume the *global decoding* scheme i.e. we set $\mathbb{F}_0 = \mathbb{F}_\tau = \emptyset$, which explains the absence

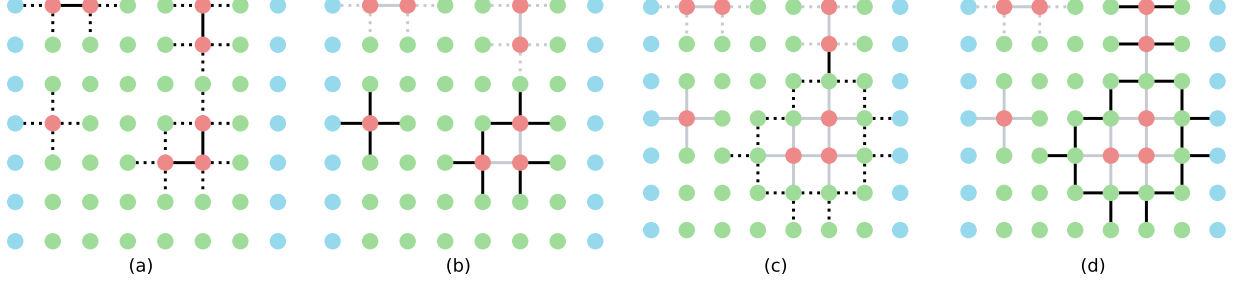


Figure 4: A syndrome validation example which needs 4 growth rounds. Ungrown edges are invisible; half-grown, dotted; fully grown, solid. Edges which have grown since the last round are black; else, grey. (a) Each defect grows its incident edges by half. Note some edges have grown by half twice, so are fully grown. (b) The two active clusters grow again. The west one touches a boundary hence inactivates. (c) The remaining active cluster grows and touches hence merges with the inactive cluster north of it. (d) The resultant active cluster grows and touches the boundary hence inactivates.

of vertical edges below ΔS_1 and above ΔS_τ in Fig. 3. This allows us to determine the success of the decoder for a batch of $\tau + 1$ measurement rounds in isolation. Considering how consecutive batches join at their time boundaries and decoding them is the topic of *sliding window decoding* which we do not treat in this paper. Global decoding, though less realistic, captures the relevant behaviour of decoders like MWPM and UF, and leads to a negligible difference in decoding accuracy [24, Appendix C].

2. We set $p = q$ which suggests τ should be on the same order as d , so we set $\tau = d$. Our versions of UF could account for $p \neq q$ by weighting the edges of G in the syndrome validation stage.

MWPM is a popular decoder which uses the following idea: for small p the number of edges in \mathbb{E} is likely to be small, so it seems sensible to minimise the number of edges in the correction. MWPM finds a correction whose size is minimal. While accurate, it has a worst-case runtime $\mathcal{O}(N^3 \lg N)$ [11, §3] where $N := |V| = \mathcal{O}(d^2)$ for perfect measurements and $\mathcal{O}(d^3)$ for faulty measurements. UF can be seen as an approximation of MWPM [28] with an improved worst-case runtime $\mathcal{O}(N\alpha(N))$ where α , the inverse of Ackermann's function, is less than three for all practical surface code distances.

For visual clarity, Fig. 4 and onwards use the graph G for perfect measurements. However, the reader should keep in mind all the material which follows (including our versions of UF) also applies to G for faulty measurements.

2.2 UF

Conceptually, UF groups defects into spatial clusters then finds a correction only from edges within a cluster. UF keeps the total size of all clusters small to ensure the correction is small. The algorithm comprises the following stages:

1. **Syndrome Validation** An active cluster nucleates at each defect which grows outward in all directions at the same speed.
2. **Spanning Forest Growth** A spanning tree is grown within each cluster. In our modification of UF, this stage comes for free.
3. **Peeling** Each edge of each tree is peeled i.e. removed from the tree and included or excluded from the correction depending on the syndrome.

2.2.1 Syndrome Validation

Figure 4 shows a syndrome validation example. Mathematically, a cluster $C = (V_C, E_C)$ is a connected subgraph of G . A cluster is *active* iff there exists no correction for its defects using only edges in the cluster i.e. $\nexists \mathbb{C} \subseteq E_C : \sigma(\mathbb{C}) = \mathbb{S} \cap V_C$. Else it is *inactive*. Intuitively, an inactive cluster is one where we have accounted for all defects with a correction local to that cluster; an active cluster still seeks such a correction. In practice we determine activity by the following lemma adapted from [3, Lemma 1] and proved in Appendix B.

Lemma 2. *Cluster C is active iff it has an odd number of defects and touches no boundary i.e.*

$$(|\mathbb{S} \cap V_C| \text{ odd}) \wedge (V_{\text{boundary}} \cap V_C = \emptyset). \quad (4)$$

Before syndrome validation, a cluster $(\{v\}, \emptyset)$ is initialised for every $v \in V$ (so there is an active cluster for each defect and an inactive one for each nondefect). Each edge in E has a *growth value* in $\{0, \frac{1}{2}, 1\}$ which is initialised at 0. Syndrome validation proceeds via some number of growth rounds and stops when all clusters are inactive. In a growth round:

1. Each active cluster grows all edges around it by a half.
2. Each new fully grown edge merges the two clusters at its endpoints into one bigger cluster, if

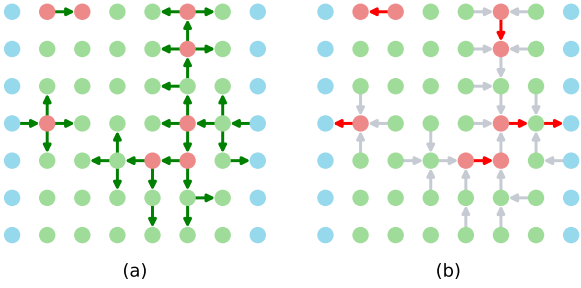


Figure 5: Continuing the example in Fig. 4: (a) A spanning forest is grown in the direction of the arrows. Each arrow is an edge in the forest and points from parent to child node. (b) The forest is peeled in the direction of the arrows. The set of red arrows is the correction returned by the decoder.

the endpoints did not already belong to the same cluster. Mathematically, if clusters A and B merge along edge e the resultant cluster is

$$C = (V_A \cup V_B, E_A \cup E_B \cup \{e\}). \quad (5)$$

One may wonder why edges grow by only half per growth round. If they grew by 1 per round, a pair of defects separated by two edges would merge just as fast as a pair separated by one edge. Growing edges by half per round distinguishes these cases, reducing the number of fully grown edges hence the size of all clusters.

Syndrome validation has a runtime $\mathcal{O}(N\alpha(N))$ if the Union–Find data structure (after which the Union–Find decoder is named) is used [26]. It ensures the *existence* of a correction using only cluster edges while the next two stages, shown in Fig. 5, find an *instance* of one.

2.2.2 Spanning Forest Growth

For each cluster C a root node is chosen as follows: if C touches a boundary, one of its boundary nodes is chosen; else, any node is chosen. A spanning tree of C (a subgraph of C that is connected, acyclic, and spans V_C) is then grown from this root. The union of all the trees is the forest. This stage is done by breadth- or depth-first search; either way, the runtime is linear in the number of edges in the forest i.e. $\mathcal{O}(N)$.

2.2.3 Peeling

A correction $\mathbb{C} = \emptyset$ is initialised then the forest is traversed edge by edge, starting from the leaves. Each time a defect is encountered all edges traversed thereafter, until another defect is encountered, are added to \mathbb{C} . Once the whole forest has been traversed \mathbb{C} will satisfy $\sigma(\mathbb{C}) = \mathbb{S}$ [4, Theorem 1]. Since each edge in the forest is traversed exactly once the runtime is $\mathcal{O}(N)$.

This concludes our review of the well-established surface code and UF paradigms, using the notation that we require for the remainder of the paper. We now briefly discuss recent literature working towards local architectures for implementing UF, especially Helios.

3 Almost-Local UF

As we can see the nature of UF is quite local: all edges involved connect neighbouring nodes, and clusters communicate with each other only when they touch; so it is natural to try to implement UF as locally as possible. This may have advantages over the standard picture in which the decoder protocol is implemented using a single, fully fledged classical processor, presumably located remotely from the actual qubits. Instead, one can imagine a more distributed decoder comprising a very simple classical processor corresponding to each node and an inter-processor communication link corresponding to each edge. We can visualise this local architecture as directly corresponding to Fig. 3(a) if nodes represent processors and edges represent the links.

This alternative paradigm has various benefits. Firstly, its computation is parallelised: non-neighbouring computations can be run independently and simultaneously; we will see later this leads to superior runtime scaling. Secondly, it is faster as each processor is simpler and sits closer to its data source (the ancilla qubit). Thirdly, there may be implications in terms of robustness: if one part breaks down then only that part, rather than the whole decoder, must be replaced.

In Section 3.1 we give a conceptual overview of Helios developed by Liyanage et al. [17] and in Section 3.2 we describe almost-local UF in detail with our modification *anyon annihilation* which simplifies the physical architecture and allows a spanning forest to be grown in 1 timestep regardless of d .

3.1 Helios

The authors consider only syndrome validation as this is the only stage that is nontrivial to implement locally. Their implementation uses the local architecture just described i.e. there is a processor for each node in G and a communication link for each edge. For the rest of this section we refer to processors as nodes and communication links as edges.

Clusters are identified by a unique integer stored by all its nodes. When two clusters merge the higher-integer cluster becomes part of the other one. This happens via a flooding algorithm: each node looks at its neighbours along fully grown edges; if it sees a lower integer than its own, it stores that lower integer instead. This results in a wave of change propagating across the higher-integer cluster, starting from where

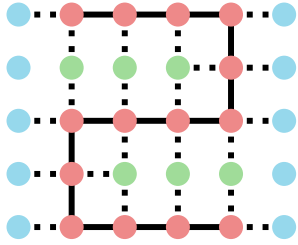


Figure 6: A maximum-length cluster is a winding snake-like path of length $\mathcal{O}(N)$ where N is the number of nodes in the graph G .

the two clusters touched. After the flood, all the nodes of the higher-integer cluster will store the lower integer. Generalising to three or more clusters merging at once is simple: a flood propagates from each touching point but eventually only the lowest-integer cluster will remain.

As well as merging, the other task in syndrome validation is determining the activity of each cluster. The authors devised the following messaging system to tackle this. Each cluster always has a well-defined root node. Whenever a defect changes its stored integer, it sends a message to the root of the cluster it has just joined. Every root stores a bit and flips it whenever it receives a message. Once all flooding has finished and all messages have reached their destination, the bit of each root will equal the parity of the number of defects in its cluster. This, by [Lemma 2](#), determines the activity of clusters which do not touch a boundary. The authors do not mention treatment of clusters which touch a boundary but we do so in [Section 3.2](#).

These messages are sent via a network of communication links comprising the edges of G and additional edges between non-neighbouring nodes [[17](#), Figure 3] but our modification removes the need for them.

In addition to the nodes, there is a single controller which manages the global variables of the UF algorithm. It connects to each node directly (in general it connects to each node indirectly via a hierarchical tree structure but for low enough code distances this tree is not used) but the type of information communicable is restricted: the controller can broadcast the same message to all nodes and receive Boolean messages from any node (but does not know which node sent the message). This controller-node connectivity is the reason we say Helios is almost local.

The worst-case runtime of Helios is $\mathcal{O}(N)$ because the maximum possible cluster length is $\mathcal{O}(N)$ (see example cluster in [Fig. 6](#)) and the duration to flood such a cluster scales linearly with its length. This is formally better than the $\mathcal{O}(N\alpha(N))$ of original UF owing to the parallelism of Helios. More impressive is the *mean* runtime which, for faulty measurements i.e. $N = \mathcal{O}(d^3)$, the authors report as sublinear in d from numerics.

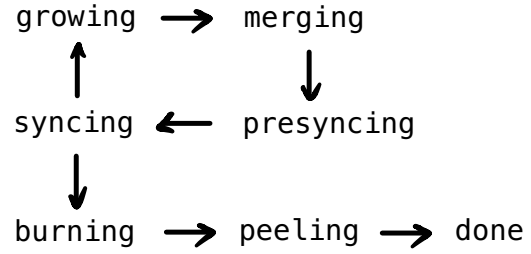


Figure 7: Flowchart for the stage variable which alternates between fixed- and arbitrary-duration stages.

3.2 Our Version of Almost-Local UF

While both Helios and our version grow clusters identically to original UF, their *final* outputs may not be identical, as \mathbb{C} depends on the choice of the root and spanning tree of each cluster. We saw however in [Fig. 1](#) this difference does not affect accuracy which is what actually matters in decoding.

We assume decoding to be cellular automata-like i.e. via discrete timesteps with each component performing one operation, and messages travelling one edge, per timestep.

The controller has a variable attribute `stage` indicating which stage it is in. It is initialised to `growing` and follows the flowchart in [Fig. 7](#). There are seven stages: `growing`, `merging`, `presyncing`, `syncing`, `burning`, `peeling`, `done`. The odd stages last exactly 1 timestep; the even stages, an arbitrary number of timesteps. During syndrome validation the controller cycles through the first four stages once per growth round. `burning` is for spanning forest growth, `peeling` is for peeling, and `done` indicates the end of the decoding cycle.

Each node is assigned a unique integer `ID` as in [Fig. 3\(a\)](#) and has the following variable attributes:

- `defect` is a boolean indicating whether the node is a defect.
- `active` is a boolean indicating whether the cluster the node is in is active. Since each node starts in its own cluster, $v.\text{active}$ is initialised as $v.\text{defect } \forall v \in V$. If $v.\text{active} = \text{true}$ we say v is active.
- `CID` is an integer indicating the cluster the node belongs to. Clusters are identified by the lowest `ID` of all its nodes. The node with this `ID` is the *root* of the cluster. $v.\text{CID}$ is initialised as $v.\text{ID } \forall v \in V$.
- `anyon` is a boolean indicating whether the node has an anyon. This anyon can be thought of as a particle which is passed between nodes during syndrome validation. When two anyons meet i.e. a node receives two anyons in a timestep, they annihilate. $v.\text{anyon}$ is initialised as $v.\text{defect } \forall v \in V$. The idea is to accumulate at the root all the

Algorithm 1 Run by controller every timestep.

```

procedure ADVANCEALMOSTLOCALCONTROLLER
  if (not  $v.\text{busy}$ )  $\forall v \in V$  then
    if stage = syncing then
      if (not  $v.\text{active}$ )  $\forall v \in V$  then
        | stage  $\leftarrow$  burning
      else
        | stage  $\leftarrow$  growing
    else
      | stage  $\leftarrow$  next stage

```

\triangleright Stage order is as introduced in [Section 3.2](#).

Algorithm 2 The four procedures each node can run during syndrome validation.

```

procedure GROWING( $v$ )
  if  $v.\text{active}$  then
    for all unfully grown edges  $e$  incident to  $v$  do
      |  $e.\text{support} \leftarrow e.\text{support} + \frac{1}{2}$ 

procedure MERGING( $v$ )
   $v.\text{busy} \leftarrow \text{false}$ 
  if ( $v \in V_{\text{bulk}}$ ) and ( $v$  not a root) and ( $v.\text{anyon}$ ) then
    |  $v.\text{busy} \leftarrow \text{true}$ 
    | relay anyon in direction of  $v.\text{pointer}$ 
  for  $u \in \text{accessibles}(v)$  do
    if  $u.\text{CID} < v.\text{CID}$  then
      |  $v.\text{busy} \leftarrow \text{true}$ 
      |  $v.\text{pointer} \leftarrow$  toward  $u$ 
      |  $v.\text{CID} \leftarrow u.\text{CID}$ 

procedure PRESYNCING( $v$ )
  |  $v.\text{active} \leftarrow (v \in V_{\text{bulk}})$  and ( $v$  a root) and ( $v.\text{anyon}$ )
```

```

procedure SYNCING( $v$ )
  |  $v.\text{busy} \leftarrow (\text{not } v.\text{active})$  and ( $\exists u \in \text{accessibles}(v) : u.\text{active}$ )
  |  $v.\text{active} \leftarrow v.\text{active}$  or  $v.\text{busy}$ 

```

anyons in a cluster so they annihilate on the way or on arrival. Eventually zero or one anyon will remain at the root, indicating the parity of the number of defects in the cluster.

- **pointer** is the direction the node should relay the anyon. Possible values (assuming faulty measurements) are C, N, W, E, S, D, U, representing centre, north, west, east, south, down, up, respectively. Following the pointers starting from any node should eventually lead to the root of the cluster it is in. Only roots have a **pointer** of C as they do not relay anyons but accumulate them. $v.\text{pointer}$ is initialised to C $\forall v \in V$. Together, **anyon** and **pointer** replace Helios' messaging system.
- **busy** is a boolean used to indicate whether the node is busy. $v.\text{busy}$ is initialised to **false** $\forall v \in V$.

Each edge has a variable attribute **support** equal to

its growth value (recall possible values are 0, $\frac{1}{2}$, 1) so $e.\text{support}$ is initialised as 0 $\forall e \in E$. Since processing is done at nodes rather than edges we can for each edge pick one of its endpoints, say the one with the lower ID, to be responsible for storing its **support**. The set of edges a node is responsible for, is then the *owned edges*

$$v.\text{owned} := \{uv : uv \in E \text{ and } v.\text{ID} < u.\text{ID}\} \quad (6)$$

stored as a constant attribute.

In each timestep the controller runs [Algorithm 1](#), which simply moves **stage** on if no node is busy. This is where the controller-node connectivity is used: the controller need not know *which* node is busy; rather, if *a* node is busy. After every **syncing** stage the controller also checks for any active clusters. If there are, another growth round is needed so **stage** is reset to **growing**. If none, syndrome validation is done so **stage** is set to **burning**.

Once **stage** reaches **done** the controller stops running [Algorithm 1](#) and the decoder outputs the correc-

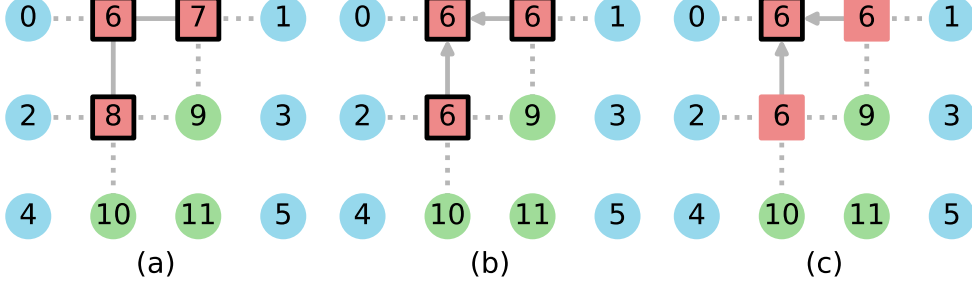


Figure 8: An example of a `merging` stage which needs 3 timesteps. Active nodes are square-shaped; inactive nodes are circular. CID is shown as a label. Nodes with anyons are outlined in black. Pointers are shown by arrows on edges. (a) The first growth stage has just finished. (b) Nodes 7 and 8 change their CID to 6 and point to node 6 which is now the root of a 3-node cluster. (c) Nodes 7 and 8 relay their anyons to the root; the two anyons annihilate and one remains, indicating the cluster has an odd number of defects. This cluster touches no boundary so by Lemma 2 is active.

tion \mathbb{C} made during peeling. In this paper we do not consider how the grid of nodes offloads \mathbb{C} and loads in the next \mathbb{S} as these are topics more relevant to sliding window decoding.

3.2.1 Syndrome Validation

It is helpful to define the *accessibles* of a node as the set of neighbours along fully grown edges:

$$\text{accessibles}(v) := \{u \in V : uv \in E \wedge uv.\text{support} = 1\}. \quad (7)$$

In a timestep each node runs whichever procedure matches `stage` out of the four in Algorithm 2.

Stage `growing` is simply a change of `supports`: each node in an active cluster increments the `support` of edges around it, if not already fully grown.

Figure 8 shows a `merging` example. In `merging` two processes happen: flooding and anyon annihilation. Flooding is as described in Section 3.1: each node looks at its accessibles; if it sees a lower CID than its own, it updates its own to match it. Additionally, the node updates its `pointer` toward that accessible. This ensures following the pointers always leads to the correct root promised by CID. In anyon annihilation, any node with an anyon relays it in the direction of its pointer. At the end of this stage, a cluster has an odd number of defects iff its root has an anyon.

Ideally, pointers are updated *before* anyons are relayed. However, the practicality of this depends on the specific hardware implementation so in this paper we assume the worse case and relay anyons in the direction of pointers from the *previous* timestep.

Stage `presyncing` determines which clusters are active. Note in Fig. 3(a) boundary nodes have lower IDs than bulk nodes. This ensures that if a cluster touches a boundary, its root is a boundary node. Each root can thus determine if its cluster is active by checking if itself is a boundary node and if it has an anyon, by Lemma 2. In `presyncing`, roots of active clusters set their `active` attribute to `true`; every other node sets

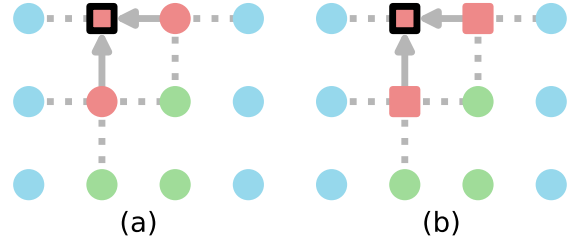


Figure 9: An example of a `syncing` stage which needs 2 timesteps. Attributes are shown as in Fig. 8 but without CID. (a) A `presyncing` stage has just finished. Note how the only active node is the root of the 3-node active cluster. (b) Nodes 7 and 8 see this active node along a fully grown edge so become active themselves. This is the end of the flood as all the nodes in the active cluster are active.

theirs to `false`.

Figure 9 shows a `syncing` example. In `syncing` the activity of each cluster is propagated from root to all its other nodes via a flood: each node looks at its accessibles; if it sees an active node, it becomes active, if not already. At the end of this stage, a node is in an active cluster iff it is active.

In Helios' messaging system, messages contain the ID of the destination node. The memory needed to store this scales logarithmically in d . A new message is emitted whenever a defect changes its CID which leads to $\mathcal{O}(N^2)$ messages throughout syndrome validation in the worst case. Messages must be kept separate so buffers are needed but these can stall if full. Anyon annihilation improves upon this system as `anyon` is a single bit regardless of d . Throughout syndrome validation, the number of anyons never exceeds the number of defects in the graph G and only ever decreases, so is $\mathcal{O}(N)$ in the worst case. There is no need for buffers (as anyons need not be kept separate) nor additional links between non-neighbouring

Algorithm 3 Run by each node during burning.

```

procedure BURNING( $v$ )
  for  $uv \in v.\text{owned}$  do
    if  $uv.\text{support} = 1$  and not ( $u.\text{pointer}$  toward  $v$  or  $v.\text{pointer}$  toward  $u$ ) then
       $uv.\text{support} \leftarrow 0$ 

```

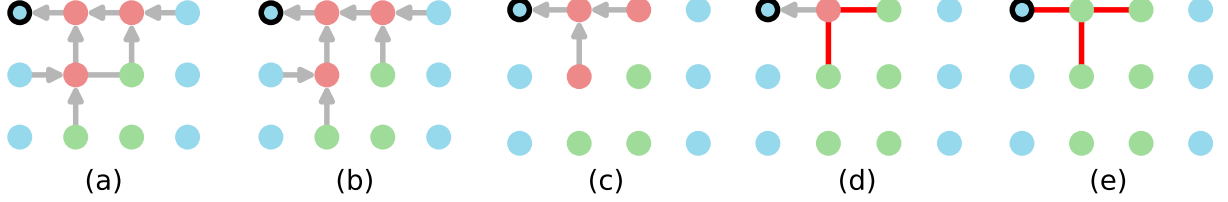


Figure 10: An example of burning and peeling. Attributes are shown as in Fig. 9. (a) Before burning, a cluster contains a cycle, which has one edge no pointer points along. (b) This edge is burned i.e. removed to leave behind a spanning forest. (c) The four leaves of the forest are peeled resulting in a smaller forest. (d) The two leaves of the smaller forest are peeled resulting in an even smaller forest. These two edges are added to the correction as the leaf nodes were defects. Edges so far added to the correction are in red. (e) The final leaf is peeled and added to the correction.

nodes.

3.2.2 Burning

In original UF a spanning forest is grown in $\mathcal{O}(N)$ timesteps via breadth- or depth-first search. Our version does this in 1 timestep by retrieving the forest directly from the pointers in a stage we call *burning*, described in Algorithm 3. An example is shown in Fig. 10(a, b). In burning, any fully grown edge no pointer points along is ‘burned’ i.e. sets its *support* to zero. The spanning forest is the set of fully grown edges which remain. This is because the pointers already define a spanning tree within each cluster; burning simply removes the edges ‘unused’ by these pointers.

3.2.3 Peeling

Algorithm 4 Run by each node during peeling.

```

procedure PEELING( $v$ )
   $v.\text{busy} \leftarrow \text{false}$ 
  if ( $v$  not a root) and ( $|\text{accessibles}(v)| = 1$ )
  then
     $v.\text{busy} \leftarrow \text{true}$ 
     $\{u\} := \text{accessibles}(v)$ 
  6:    $uv.\text{support} \leftarrow 0$ 
    if  $v.\text{defect}$  then
      8:      $v.\text{defect} \leftarrow \text{false}$ 
      add  $uv$  to  $\mathcal{C}$ 
      flip  $u.\text{defect}$ 

```

Figure 10(b–e) shows our version of peeling which is simply a local version of that described in Sec-

tion 2.2.3 and takes $\mathcal{O}(N)$ timesteps. In a timestep each node runs the procedure in Algorithm 4: each node checks if it is a leaf node of the spanning forest; if so it will peel its corresponding leaf edge.

3.2.4 Worst-Case Runtime Scaling

Our version’s worst-case decoding runtime is $\mathcal{O}(N)$ due to the same reason as Helios’: flooding a cluster of length $\mathcal{O}(N)$ is the process with the worst scaling in the whole decoding cycle. Specifically, the number of timesteps to flood a cluster equals its length in edges. We expect mean runtime to scale almost identically to Helios’ which we indeed observe in Section 5.

4 Strictly Local UF

We now present a version of UF without a direct communication link between the controller and each node. Instead, the controller communicates only with the node whose ID is 0. Broadcasting of *stage* from controller to nodes happens via a flood through the whole graph G , and *busy* and *active* propagate as signals from node to controller by relaying. We call these two new processes *staging* and *signalling*, respectively. Signalling is similar to how anyons are relayed but instead of being relayed along pointers these signals are simply relayed toward the controller, one edge per timestep. This requires the controller and nodes to store additional attributes which are described in Section 4.1.

The change clearly increases runtime but has the advantage of lacking long-range links, so is an even lower stepping stone toward practicality. The worst-case runtime remains $\mathcal{O}(N)$ and is discussed in Sec-

tion 4.3. We will see in Section 5 that the mean runtime stays below $\mathcal{O}(d^2)$ for physical error probabilities below threshold (recall from Section 2.1.1 this is the decoder’s operable region). Moreover we presently note that a rapid-transmission variant can substantially recover the speed of the almost-local architecture within the strictly local paradigm.

4.1 Additional Attributes

The controller stores a constant integer `span` which equals the number of edges to the furthest node. This node is always the boundary node with the highest ID e.g. node 17 in Fig. 3(a). The controller also has the following variable attributes:

- `countdown` is an integer which tracks how long the controller must wait until it is sure staging or signalling is done. It is initialised to 0.
- `busy_signal` is a boolean indicating whether the controller receives a `busy_signal` in the current timestep.
- `active_signal` is a boolean indicating whether the controller *has* received an `active_signal` during the current `syncing` stage. It is initialised to `false`.

Each node stores the following constants:

- `span` is an integer which equals the number of edges from itself to the node furthest from the controller.
- `signalee` is the neighbour in the direction toward the controller. This is the neighbour the node looks to for staging, and sends `busy_signals` and `active_signals` to. For faulty measurements: it equals the neighbour below; if the node is already in the lowest sheet ΔS_1 , it is instead the east neighbour; if the node is already eastmost, it is instead the north neighbour. For node 0, `signalee` is the controller.

Each node also has the following variable attributes:

- `stage` is same as that of controller. This is used for staging and is initialised to `growing` $\forall v \in V$.
- `countdown` is same as that of controller but used only to track how long the node must wait until staging is done. It is initialised to 0 $\forall v \in V$.
- `busy_signal` is a boolean indicating if in the current timestep the node either is busy or receives a `busy_signal` from another node.
- `active_signal` is a boolean indicating if in the current timestep the node either has `stage` as `presyncing` and becomes active or receives an `active_signal` from another node.

To manage these additional attributes the procedures have additional steps. These are explained in the next subsection.

4.2 Modified Procedures

For the controller, Algorithm 1 is replaced by Algorithm 5. Main differences are: checking for any busy nodes is replaced by checking if `countdown` has reached zero; checking for any active nodes, by checking if an `active_signal` has been received.

Algorithm 5 Run by controller every timestep in strictly local UF.

```

procedure ADVANCELOCALCONTROLLER
2:   if countdown = 0 then
4:     > stage change block.
      if stage = syncing then
6:        if not active_signal then
          | stage  $\leftarrow$  burning
        else
8:          | stage  $\leftarrow$  growing
      else
10:        | stage  $\leftarrow$  next stage
        > countdown reset block.
12:        if stage  $\in \{\text{merging, peeling}\} then
          | countdown  $\leftarrow$  span + 1
14:        else
          | countdown  $\leftarrow$  span
16:      else if busy_signal and countdown  $\in \{1, 2\}$ 
18:      then
          | countdown  $\leftarrow$  2 > Only happens during
            arbitrary-duration stages.
        else
          | countdown  $\leftarrow$  countdown - 1$ 
```

In Section 3.2 the four stages that lasted 1 timestep each follow an arbitrary-duration stage, so in SLUF, staging must be used to broadcast these four stages to the nodes. As indicated in Line 15 it takes `span` timesteps for staging to complete i.e. for a `stage` flood to propagate from controller to the furthest node. Hence these four stages are still of fixed duration (for a fixed d).

The other three (arbitrary-duration) stages need not be broadcast as they each follow a fixed-duration stage so the nodes know exactly when to start them. In `merging` and `peeling` the controller must wait at least `span` + 1 timesteps as it takes `span` timesteps for a signal to go from the furthest node to the controller. Line 13 indicates this. In `syncing` the furthest node (a boundary node) is never busy nor active so the controller need only wait at least `span` timesteps (Line 15). In any of these three stages, after this minimum duration, `busy_signals` are no more than 2 edges apart due to Proposition 1 so `countdown` resets to 2 in Line 17.

Algorithm 6 Each node in strictly local UF runs ADVANCELOCALNODE every timestep.

```

procedure ADVANCELOCALNODE( $v$ )
2:   PROC  $\leftarrow$  procedure matching  $v.\text{stage}$  in Algorithms 2 to 4
   if  $v.\text{stage} \in \{\text{merging, syncing, peeling}\}$  then
4:     ADVANCEARBITRARY( $v$ , PROC)
   else
6:     ADVANCEFIXED( $v$ , PROC)

8: procedure ADVANCEFIXED( $v$ , PROC) ▷ For fixed-duration stages.
   if  $v.\text{countdown} = 0$  then
10:    PROC( $v$ )
    if  $v.\text{stage} = \text{presyncing}$  then
12:       $v.\text{active\_signal} \leftarrow v.\text{active}$ 
       $v.\text{stage} \leftarrow \text{next stage}$ 
14:    else
       $\text{countdown} \leftarrow \text{countdown} - 1$ 

16: procedure ADVANCEARBITRARY( $v$ , PROC) ▷ For arbitrary-duration stages.
18:   if  $v.\text{stage} = v.\text{signalee.stage}$  then
19:     PROC( $v$ )
20:      $v.\text{busy\_signal} \leftarrow v.\text{busy\_signal}$  or  $v.\text{busy}$ 
     relay  $v.\text{busy\_signal}$  and  $v.\text{active\_signal}$  to  $v.\text{signalee}$ 
22:   else
      $v.\text{stage} \leftarrow v.\text{signalee.stage}$  ▷ Staging.
24:    $v.\text{countdown} \leftarrow v.\text{span}$ 

```

Proposition 1 (Doppler effect). *For any `busy_signal` received by the controller after $\text{span} + 1$ timesteps in `merging`, another `busy_signal` must have been received ≤ 2 timesteps earlier.*

Proof. All `busy_signals` emitted in the first `merging` timestep reach the controller in $\text{span} + 1$ timesteps or less. Hence any `busy_signal` s received after this time must have been emitted by some node v at some time t_s after the first `merging` timestep. This implies at $t_s - 1$ some node $u \in \{v\} \cup \text{accessibles}(v)$ was busy, so emitted a `busy_signal` s' . The duration between the controller receiving s' and s is maximised when u is one edge closer to the controller than v . In this case s' arrives 2 timesteps before s . \square

The proof of [Proposition 1](#) can be understood as a Doppler effect: waves of busyness travel through clusters at a speed of 1 edge per timestep. Wavefronts emit `busy_signals` at a frequency of 1 per timestep. If a wave travels away from the controller, the controller will receive these signals at a frequency of 1 per 2 timesteps.

In a timestep each node runs ADVANCELOCALNODE in [Algorithm 6](#). This reuses [Algorithms 2 to 4](#) but wraps each procedure in either ADVANCEFIXED or ADVANCEARBITRARY depending on whether the stage is of fixed or arbitrary duration.

A node's `countdown` is used only when its `stage` is of fixed duration, during which it should equal the controller's `countdown`. It tells the node exactly when to change `stage`: as soon as it reaches zero in [Line 9](#).

At other times i.e. after arbitrary-duration stages, the update of `stage` happens via staging ([Line 23](#)).

4.3 Worst-Case Runtime Scaling

The new processes in SLUF, staging and signalling, take $\mathcal{O}(d)$ timesteps and are used $\mathcal{O}(1)$ times per growth round. A decoding cycle needs a maximum of $\mathcal{O}(d)$ growth rounds so these processes contribute a maximum $\mathcal{O}(d^2)$ timesteps to the overall runtime. This scaling does not exceed $\mathcal{O}(N)$ regardless of whether $N = \mathcal{O}(d^2)$ or $\mathcal{O}(d^3)$ so the worst-case runtime scaling of SLUF remains $\mathcal{O}(N)$.

5 Runtime Data

We test the runtime of our version of almost-local UF (ALUF) and SLUF by emulating many decoding cycles and counting the number of timesteps to complete syndrome validation. This is a good proxy for decoding runtime as we already know the exact runtime of burning, and the runtime of peeling equals the length of the longest cluster which is at most the runtime of the last round of merging.

In fact, `burning` and `peeling` need not be standalone stages. We could have incorporated peeling into merging if, instead of relaying an anyon along an edge, we peeled that edge, with the modifications in [Algorithm 4](#) that [Line 6](#) is not done and [Line 9](#) becomes $\mathbb{C} \leftarrow \mathbb{C} \Delta \{uv\}$. Defects would then take over

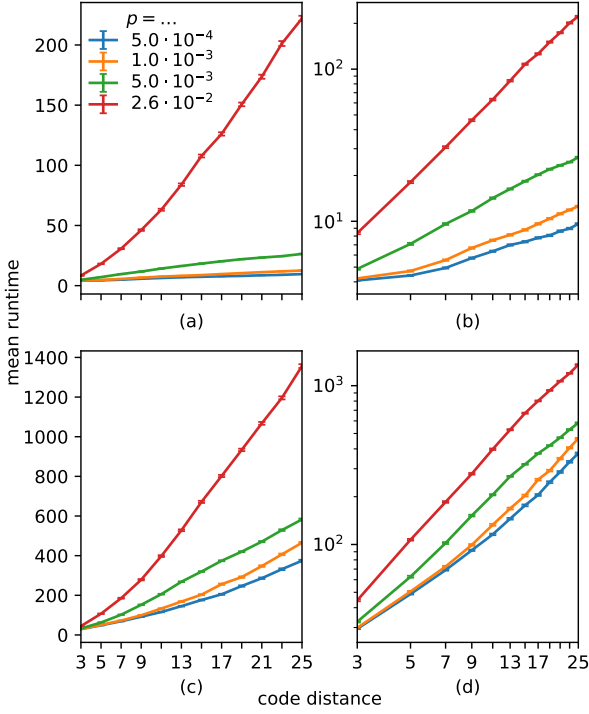


Figure 11: Mean runtime to complete syndrome validation against code distance for four different physical error probabilities p (we set measurement error probability $q = p$). Each datapoint is the mean of 10^3 samples of decoding cycle, with errorbars showing standard error. (a) Almost-local UF. (b) Same as (a) but on a log–log scale. (c) Strictly local UF. (d) Same as (c) but on a log–log scale.

the role of anyons and the decoding cycle would finish after the last `syncing` stage, without need for burning. Although small, this modification may be useful in future implementations for which we want to minimise the number of stages e.g. a sliding window local UF.

Figure 11 shows the mean runtime for both versions of UF. The gradients of the best-fit lines for the log–log plots (b, d) estimate the mean runtime scaling with code distance. These are tabulated in Table 1. Note $p = 2.6 \cdot 10^{-2}$ is the threshold of UF so $5.0 \cdot 10^{-3}$ is roughly the highest practical p at which UF would operate. For this value of p and below: ALUF shows sublinear scaling; SLUF, subquadratic scaling. We expect the former as ALUF is closely related to Helios which Liyanage et al. [17] observe to have sublinear scaling.

As well as the mean, we also evaluate the distribution of runtimes which are shown in Figs. 12 and 13. SLUF has equally spaced sharp peaks in runtime; each one corresponds to a certain number of growth rounds. The wide spacing implies most of the runtime is due to staging and signalling i.e. the controller waiting until countdown reaches zero before moving on [this can also be inferred by the difference in abso-

Table 1: The best estimate of m such that the mean runtime $\propto d^m$ where d is code distance.

p	almost-local UF	strictly local UF
$5.0 \cdot 10^{-4}$	0.35(2)	1.09(2)
$1.0 \cdot 10^{-3}$	0.48(3)	1.21(4)
$5.0 \cdot 10^{-3}$	0.83(1)	1.39(3)
$2.6 \cdot 10^{-2}$	1.61(1)	1.63(3)

lute runtime between ALUF (which does not need a countdown) and SLUF: at $d = 25$ the former is more than 20 times faster than the latter]. The countdown start, hence the peak spacing, increases linearly with d .

The peak locations can be derived as follows. If syndrome validation comprises 0 or 1 growth rounds, `countdown` resets to `span` or `span` + 1 three times (see Fig. 7). For 2 growth rounds, `countdown` resets seven times. For $r \geq 0$ growth rounds, `countdown` resets $\max\{3, 4r - 1\}$ times. Hence the peak corresponding to r growth rounds is roughly located at $\text{span} \cdot \max\{3, 4r - 1\}$ timesteps.

6 Asynchronous Logic

As just mentioned, most of the runtime of SLUF is due to staging and signalling (defined in Section 4). The fraction of runtime spent on these operations for the realistic scenario of $p = 5.0 \cdot 10^{-3}$ and $d = 25$, is 0.955.

This motivates the question: can we recover the speed of ALUF whilst maintaining strict locality? So far we have only considered versions of UF in which each node changes its state once per timestep, based on states in previous timesteps. Signals between nodes therefore are limited to travel at one edge per timestep. A timestep would correspond to *at least* one clock cycle of an FPGA or ASIC implementation of the algorithms described in this paper. However, for the information relayed by staging and signalling and the registers they effect, it is possible for each node to change the state of said registers *asynchronously* i.e. as soon as it receives the information to do so without having to wait for a timestep to complete.

This has one clear advantage, and a secondary one. Primarily, it is faster: signal speed is limited only by how fast each node responds to its inputs. This speed advantage is greatest if used for simple, indiscriminate operations like staging and signalling. The secondary benefit is that the logic overhead is likely lower as the number of registered, i.e. clocked, signals is fewer and consequently less heat is generated.

Therefore, it makes sense to consider a strictly local version of UF which uses unregistered signals relayed via buffers and/or combinational logic for staging and signalling, and traditional synchronous logic (based

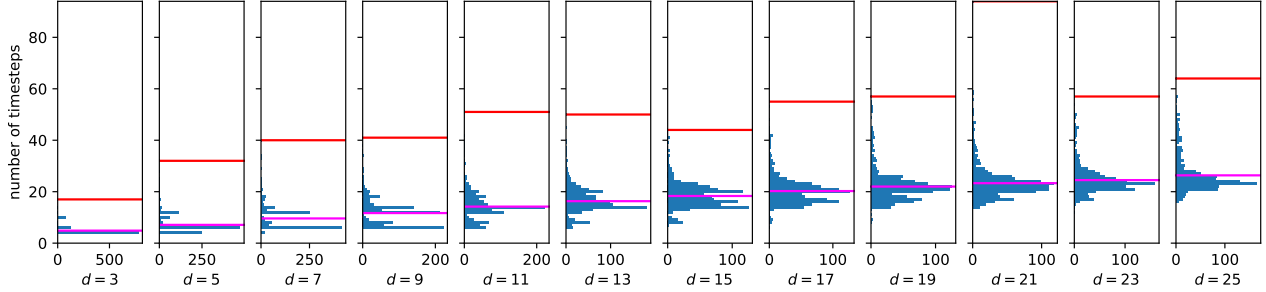


Figure 12: Distribution of runtime to complete syndrome validation using almost-local UF, for physical error probability $p = 5.0 \cdot 10^{-3}$. Within each histogram: the horizontal magenta line shows the mean; red line, the maximum, of 10^3 samples of decoding cycle. Each bar has width 1.

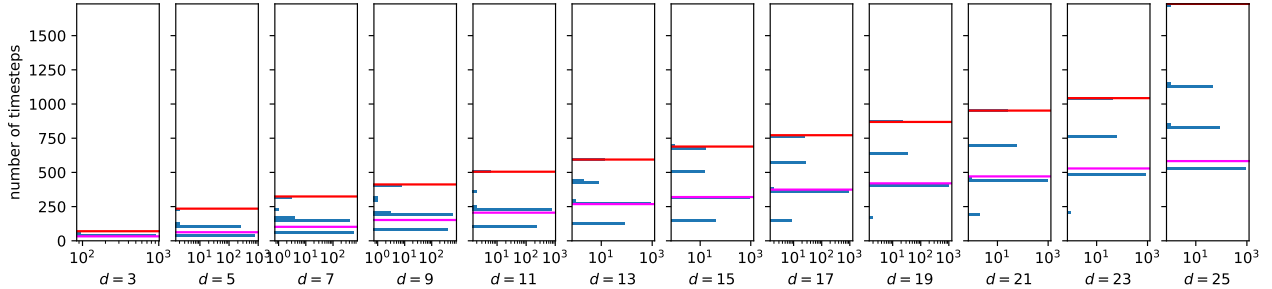


Figure 13: Same as Fig. 12 but for strictly local UF. Each bar has width 21. Note the x -axes show counts on a log scale.

on the algorithm timesteps) for all other operations. In the case that it takes less than one synchronous clock cycle for a signal to travel across the whole array via this technique, the runtime will be identical to ALUF whilst maintaining strict locality.

We stress that within our SLUF paradigm, staging and signalling are ideally suited to implementation with unregistered signals spanning the array, since there is no risk of race conditions leading to indeterminate behaviour. The signals travel through the array in such a fashion that it does not matter if propagation along one path is faster or slower than an alternate; we need only understand the timescale for the process to be complete.

7 Conclusion

We explore UF realised by local architectures, following recent developments including the Helios implementation [17]. We present an improved ‘almost-local’ model, and moreover a new, extremely practical, implementation that is strictly local; the first of its kind. We numerically reproduce the sublinear in d mean runtime scaling of Helios then observe a sub-quadratic scaling for our strictly local variant; both are better than the slightly higher-than-cubic scaling of original UF. Further, we note our strictly local paradigm is compatible with the use of asynchronous logic to massively speed up runtime without sacrificing locality, making it an attractive design option.

8 Acknowledgements

We thank Armands Strikis and David Garner for useful discussions. The authors would like to acknowledge the use of the University of Oxford Advanced Research Computing (ARC) facility [22] in carrying out this work and specifically the facilities made available from the EPSRC QCS Hub grant (agreement No. EP/T001062/1). The authors also acknowledge support from EPSRC’s Robust and Reliable Quantum Computing (RoaRQ) project (EP/W032635/1). TC acknowledges an EPSRC DTP studentship. Open-source Python libraries used in this work include `matplotlib`, `networkx`, `pytest`, `scipy`, `pandas`, `statsmodels`.

9 Author Contributions

SCB contributed to the core concepts for ALUF/SLUF, and authored elements of the paper. TC established the core concepts ALUF/SLUF, implemented, tested and validated these concepts, wrote the emulation code, collected and processed the numerical data, and was the primary author of the paper.

Note added: At the time of submission of this preprint, we noted that Ref. [17] had recently been updated to incorporate a concept comparable to our pointer mechanism. The revised version of [17] notes

the advantages versus its earlier messaging system, which we allude to in our discussions of this work.

References

- [1] Ben Criger and Imran Ashraf. Multi-path summation for decoding 2D topological codes. *Quantum*, 2:102, October 2018. [doi:10.22331/q-2018-10-19-102](https://doi.org/10.22331/q-2018-10-19-102).
- [2] Nicolas Delfosse. Hierarchical decoding to reduce hardware requirements for quantum computing, 2020. [arXiv:2001.11427](https://arxiv.org/abs/2001.11427).
- [3] Nicolas Delfosse and Naomi H. Nickerson. Almost-linear time decoding algorithm for topological codes. *Quantum*, 5:595, December 2021. [doi:10.22331/q-2021-12-02-595](https://doi.org/10.22331/q-2021-12-02-595).
- [4] Nicolas Delfosse and Gilles Zémor. Linear-time maximum likelihood decoding of surface codes over the quantum erasure channel. *Physical Review Research*, 2:033042, July 2020. [doi:10.1103/PhysRevResearch.2.033042](https://doi.org/10.1103/PhysRevResearch.2.033042).
- [5] Eric Dennis, Alexei Kitaev, Andrew Landahl, and John Preskill. Topological quantum memory. *Journal of Mathematical Physics*, 43(9):4452–4505, September 2002. [doi:10.1063/1.1499754](https://doi.org/10.1063/1.1499754).
- [6] Guillaume Duclos-Cianci and David Poulin. Fast decoders for topological quantum codes. *Physical Review Letters*, 104:050504, February 2010. [doi:10.1103/PhysRevLett.104.050504](https://doi.org/10.1103/PhysRevLett.104.050504).
- [7] Guillaume Duclos-Cianci and David Poulin. A renormalization group decoding algorithm for topological quantum codes. In *2010 IEEE Information Theory Workshop*, pages 1–5, August 2010. [doi:10.1109/CIG.2010.5592866](https://doi.org/10.1109/CIG.2010.5592866).
- [8] Jack Edmonds. Paths, trees, and flowers. *Canadian Journal of Mathematics*, 17:449–467, 1965. [doi:10.4153/CJM-1965-045-4](https://doi.org/10.4153/CJM-1965-045-4).
- [9] Austin G. Fowler, Matteo Mariantoni, John M. Martinis, and Andrew N. Cleland. Surface codes: Towards practical large-scale quantum computation. *Physical Review A*, 86:032324, September 2012. [doi:10.1103/PhysRevA.86.032324](https://doi.org/10.1103/PhysRevA.86.032324).
- [10] Austin G. Fowler, Adam C. Whiteside, and Lloyd C. L. Hollenberg. Towards practical classical processing for the surface code. *Physical Review Letters*, 108:180501, May 2012. [doi:10.1103/PhysRevLett.108.180501](https://doi.org/10.1103/PhysRevLett.108.180501).
- [11] Oscar Higgott. PyMatching: A Python package for decoding quantum codes with minimum-weight perfect matching. *ACM Transactions on Quantum Computing*, 3(3):1–16, June 2022. [doi:10.1145/3505637](https://doi.org/10.1145/3505637).
- [12] Oscar Higgott, Thomas C Bohdanowicz, Aleksander Kubica, Steven T Flammia, and Earl T Campbell. Fragile boundaries of tailored surface codes and improved decoding of circuit-level noise, 2022. [arXiv:2203.04948](https://arxiv.org/abs/2203.04948).
- [13] Oscar Higgott and Nikolas P. Breuckmann. Improved single-shot decoding of higher dimensional hypergraph product codes, 2022. [doi:10.48550/ARXIV.2206.03122](https://doi.org/10.48550/ARXIV.2206.03122).
- [14] Shui Hu. *Quasilinear Time Decoding Algorithm for Topological Codes with High Error Threshold*. PhD thesis, Delft University of Technology, June 2020. [doi:10.13140/RG.2.2.13495.96162](https://doi.org/10.13140/RG.2.2.13495.96162).
- [15] Kao-Yueh Kuo and Ching-Yi Lai. Exploiting degeneracy in belief propagation decoding of quantum codes. *npj Quantum Information*, 8(1):111, September 2022. [doi:10.1038/s41534-022-00623-2](https://doi.org/10.1038/s41534-022-00623-2).
- [16] Daniel Litinski. A game of surface codes: Large-scale quantum computing with lattice surgery. *Quantum*, 3:128, March 2019. [doi:10.22331/q-2019-03-05-128](https://doi.org/10.22331/q-2019-03-05-128).
- [17] Namitha Liyanage, Yue Wu, Alexander Deters, and Lin Zhong. Scalable quantum error correction for surface codes using FPGA, 2023. [arXiv:2301.08419](https://arxiv.org/abs/2301.08419).
- [18] Kai Meinerz, Chae-Yeun Park, and Simon Trebst. Scalable neural decoder for topological surface codes. *Physical Review Letters*, 128:080505, February 2022. [doi:10.1103/PhysRevLett.128.080505](https://doi.org/10.1103/PhysRevLett.128.080505).
- [19] Michael A. Nielsen and Isaac L. Chuang. *Quantum Computation and Quantum Information: 10th Anniversary Edition*. Cambridge University Press, 2010. [doi:10.1017/CBO9780511976667](https://doi.org/10.1017/CBO9780511976667).
- [20] Ramon W. J. Overwater, Masoud Babaie, and Fabio Sebastian. Neural-network decoders for quantum error correction using surface codes: A space exploration of the hardware cost-performance tradeoffs. *IEEE Transactions on Quantum Engineering*, 3:1–19, May 2022. [doi:10.1109/TQE.2022.3174017](https://doi.org/10.1109/TQE.2022.3174017).
- [21] Gokul Subramanian Ravi, Jonathan M. Baker, Arash Fayyazi, Sophia Fuhui Lin, Ali Javadi-Abhari, Massoud Pedram, and Frederic T. Chong. Better than worst-case decoding for quantum error correction, 2022. [arXiv:2208.08547](https://arxiv.org/abs/2208.08547).
- [22] Andrew Richards. *University of Oxford Advanced Research Computing*, August 2015. [doi:10.5281/zenodo.22558](https://doi.org/10.5281/zenodo.22558).
- [23] Milap Sheth, Sara Zafar Jafarzadeh, and Vlad Gheorghiu. Neural ensemble decoding for topological quantum error-correcting codes. *Physical Review A*, 101:032338, March 2020. [doi:10.1103/PhysRevA.101.032338](https://doi.org/10.1103/PhysRevA.101.032338).
- [24] Luka Skoric, Dan E Browne, Kenton M Barnes, Neil I Gillespie, and Earl T Campbell. Parallel window decoding enables scalable fault tolerant quantum computation, 2023. [arXiv:2209.08552](https://arxiv.org/abs/2209.08552).
- [25] Samuel C. Smith, Benjamin J. Brown, and Stephen D. Bartlett. Local predecoder to reduce

the bandwidth and latency of quantum error correction. *Physical Review Applied*, 19:034050, March 2023. [doi:10.1103/PhysRevApplied.19.034050](https://doi.org/10.1103/PhysRevApplied.19.034050).

[26] Robert Endre Tarjan. Efficiency of a good but not linear set union algorithm. *Journal of the ACM*, 22(2):215–225, April 1975. [doi:10.1145/321879.321884](https://doi.org/10.1145/321879.321884).

[27] James R. Wootton and Daniel Loss. High threshold error correction for the surface code. *Physical Review Letters*, 109:160503, October 2012. [doi:10.1103/PhysRevLett.109.160503](https://doi.org/10.1103/PhysRevLett.109.160503).

[28] Yue Wu, Namitha Liyanage, and Lin Zhong. An interpretation of union-find decoder on weighted graphs, 2022. [arXiv:2211.03288](https://arxiv.org/abs/2211.03288).

A Proof of Lemma 1

First consider the following.

Lemma 3 (Distributivity of σ). *The syndrome of the symmetric difference of errors is the symmetric difference of their syndromes i.e. for $n \geq 2$:*

$$\sigma\left(\bigtriangleup_{i=1}^n \mathbb{E}_i\right) = \bigtriangleup_{i=1}^n \sigma(\mathbb{E}_i). \quad (8)$$

Proof. By induction. Consider base case $n = 2$:

$$\sigma(\mathbb{E}_1 \Delta \mathbb{E}_2) \stackrel{(1)}{=} V_{\text{bulk}} \cap \bigtriangleup_{e \in \mathbb{E}_1 \Delta \mathbb{E}_2} e. \quad (9)$$

Since $e \Delta e \equiv \emptyset$ we have $\bigtriangleup_{e \in \mathbb{E}_1 \Delta \mathbb{E}_2} e \equiv (\bigtriangleup_{e \in \mathbb{E}_1} e) \Delta (\bigtriangleup_{e \in \mathbb{E}_2} e)$ so

$$\sigma(\mathbb{E}_1 \Delta \mathbb{E}_2) \stackrel{(1)}{=} \sigma(\mathbb{E}_1) \Delta \sigma(\mathbb{E}_2) \quad (10)$$

so true for $n = 2$. Now for the inductive step; assume true for $n = k$ and consider for $n = k + 1$:

$$\begin{aligned} \bigtriangleup_{i=1}^{k+1} \mathbb{E}_i &= \left(\bigtriangleup_{i=1}^k \mathbb{E}_i \right) \Delta \mathbb{E}_{k+1} \\ \sigma\left(\bigtriangleup_{i=1}^{k+1} \mathbb{E}_i\right) &\stackrel{(10)}{=} \sigma\left(\bigtriangleup_{i=1}^k \mathbb{E}_i\right) \Delta \sigma(\mathbb{E}_{k+1}) \\ &\stackrel{(8)}{=} \bigtriangleup_{i=1}^{k+1} \sigma(\mathbb{E}_i). \end{aligned} \quad (11)$$

Hence, true for $n = k$ implies true for $n = k + 1$. Together, the base case and inductive step imply true for $n \geq 2$. \square

Now we can prove Lemma 1.

Proof of Lemma 1. Consider the syndrome produced by the leftover:

$$\begin{aligned} \sigma(\mathbb{L}) &\stackrel{(10)}{=} \sigma(\mathbb{E}) \Delta \sigma(\mathbb{C}) \\ &= \mathbb{S} \Delta \mathbb{S} \\ &= \emptyset. \end{aligned} \quad (12)$$

Hence, every bulk node is incident to an even number of edges in \mathbb{L} . This can only happen if \mathbb{L} comprises cycles or paths whose endpoints are both boundary nodes. Since each boundary node is incident to exactly one edge and \mathbb{L} comprises distinct edges, these endpoints must be distinct. \square

B Proof of Lemma 2

We prove the following equivalent statement.

Lemma 4. *Cluster C is inactive iff it has an even number of defects or touches a boundary i.e.*

$$(|\mathbb{S} \cap V_C| \text{ even}) \vee (V_{\text{boundary}} \cap V_C \neq \emptyset). \quad (13)$$

Proof.

\Rightarrow We know $\exists \mathbb{C} \subseteq E_C : \sigma(\mathbb{C}) = \mathbb{S} \cap V_C$. If C touches...

- no boundary, $|\sigma(\mathbb{C})|$ even $\forall \mathbb{C} \subseteq E_C$ as adding any edge in E_C to \mathbb{C} changes $|\sigma(\mathbb{C})|$ by either 0 or 2.
- a boundary, $|\sigma(\mathbb{C})|$ can be even or odd as adding an edge containing a boundary node to \mathbb{C} changes $|\sigma(\mathbb{C})|$ by 1.

\Leftarrow If $|\mathbb{S} \cap V_C|$ even, partition $\mathbb{S} \cap V_C$ into $s/2$ pairs where $s := |\mathbb{S} \cap V_C|$. C connected so there exists a path $P_i \subseteq E_C$ between the defects in each pair. Be $\mathbb{C} := \bigtriangleup_{i=1}^{s/2} P_i$ the symmetric difference of these paths then

$$\sigma(\mathbb{C}) \stackrel{(8)}{=} \bigtriangleup_{i=1}^{s/2} \sigma(P_i) \quad (14)$$

where $\sigma(P_i)$ is precisely the i^{th} pair so

$$\begin{aligned} \sigma(\mathbb{C}) &= \bigcup_{i=1}^{s/2} \sigma(P_i) \\ &= \mathbb{S} \cap V_C. \end{aligned} \quad (15)$$

The existence of a correction satisfying Eq. (15) is the definition for C to be inactive.

If $|\mathbb{S} \cap V_C|$ odd, C must touch a boundary so pick any boundary node $v \in V_C$. Partition $(\mathbb{S} \cap V_C) \cup \{v\}$ into $s/2$ pairs where $s := |(\mathbb{S} \cap V_C) \cup \{v\}|$. Once again there exists a path P_i between the nodes in each pair so construct \mathbb{C} as before then Eqs. (14) and (15) follow. \square